Article

Experimental Study of the Influence of Rotor Dynamics on the Temperature Distribution of a Gas Foil Bearing

Paweł Bagiński [1,*], Grzegorz Żywica [1], Jakub Roemer [2,3], Paweł Zdziebko [2] and Adam Martowicz [2]

[1] Department of Turbine Dynamics and Diagnostics, Institute of Fluid-Flow Machinery, Polish Academy of Sciences, Fiszera 14, 80-231 Gdansk, Poland

[2] Department of Robotics and Mechatronics, AGH University of Science and Technology, al. Mickiewicza 30, 30-059 Krakow, Poland

[3] Department of Mechanical, Electronics and Chemical Engineering, Oslo Met-Oslo Metropolitan University, Postboks 4, Street Olavs Plass, 0130 Oslo, Norway

[*] Correspondence: pbaginski@imp.gda.pl

Abstract: This article presents an experimental study carried out on a rotor operating on two foil bearings. One of the bearings was built in a way to measure the temperature and deformation of the top foil of the foil bearing. The dynamic performance of the two bearing journals is presented herein using the vibration trajectories and journal positions in the foil bearing sleeve. Based on these results, a method for predicting the temperature distribution on the top foil was developed. Then, the correlations between the temperature distribution and the operating parameters of the bearing journal were illustrated. It has been observed that the symmetry of the temperature distribution on the top foil depends on the eccentricity of the rotor operation. The shape and size of the vibration trajectory had no significant effect on the temperature value in the bearing, unlike the position of the journal in the bearing. The process of loss of the gas lubricating film was observed, which provides insight into the phenomena that occur during the first few seconds of rotor operation. The areas in the bearing from which fresh air had been drawn into the gap between the journal and the top foil were also determined.

Keywords: foil bearings; journal bearings; oil-free bearings; dynamic characteristic; thermal management

1. Introduction

As it is known, the use of specific bearings in a machine is usually determined by the operating conditions of the machine, such as the weight of the shaft and its speed, the ecological nature of the lubricant used for the bearings, the operating temperature range of the machine, etc. One type of gas bearing is the foil bearing, best suited for low loads and high rotational speeds [1]. Some companies are trying to introduce devices that use foil bearings, as these are becoming better designed. What has contributed to this is the enormous work of scientists around the world who have performed numerous experiments and simulations to study the phenomena that occur in foil bearings. The main parameters in these types of bearings are the stiffness and damping of the foil assembly [2] (bump foil and top foil), which largely depend on the material they are made of [3], the shape of the bumps [4], as well as the friction pair selected for the journal and top foil [5,6]. These parameters and the correlations between them have already been well studied (although some aspects still need to be tested), and some numerical and theoretical models can predict them with a very good accuracy [7]. The ever-increasing computing power of computers has led to the creation of 3D numerical models that combine the deformation of the support structure caused by the pressure exerted by air in the bearing and, at the same time, the deformation of the lubricating film caused by the deformation of the foil assembly (via FSI—Fluid Structure Interaction) [8]. Another parameter that determines the proper operation of the foil bearing is the temperature of the gas film [9]. This important information

has been neglected for some time because, in traditional gas bearings, small temperature fluctuations were assumed not to affect bearing operation, so isothermal models were used in the calculations [10]. It is important to note that a foil bearing is not an ordinary gas bearing as it has additional components between the journal and the sleeve that determine the operating performance of the bearing and its variable lubrication gap, which is associated with the temperature that is generated [11,12].

There are experimental studies that confirm the non-isothermal nature of the operation of the foil bearing [13]. The very fact that the journal in a foil bearing begins to rotate under conditions of dry friction, then viscous friction and then is isolated by the air film formed, confirms the need to monitor the temperature of components that are at risk of damage (such as the top foil). In experimental studies, the number of temperature sensors used to monitor the proper operation of the bearing varies from one to several. In some studies, the temperature is specifically raised to several hundred degrees Celsius in order to investigate the capabilities of foil bearings and try to find ways how to cool them effectively [14]. All these studies require numerical and theoretical models capable of predicting the temperature value and, more importantly, its distribution on the top foil, with respect to the other operating parameters of the rotor [15]. Practically, the lubrication gap cannot be effectively cooled or flushed since we do not know how the cool air suction mechanism between the journal and the top foil works, and what the external and internal factors of the system that determine the temperature rise are. The authors undertook the difficult task of experimentally investigating the temperature distribution on the surface of the bump foil, something that has not been often covered in the literature to date. There are research papers that describe the effect of journal dynamics on the temperature in the bearing at the measuring points, but this has not been able to explain the temperature distribution on the top foil. There are many numerical works that show such a distribution on the top foil, but they have not yet been verified. The results of this work will allow the numerical models to be correctly verified and will also help to develop a method for measuring the temperature and its distribution on the top foil.

The authors of this article have provided a detailed description of a foil bearing, which was designed to measure the temperature and deformation of the top foil depending on the rotational speed, bearing load, eccentricity and rotor dynamics. The article gives information on the temperature of the top foil recorded under various operating conditions of the bearing, from which its distribution was created. In addition, the basic dynamic parameters of the rotor operating on foil bearings have been presented. The authors determined the correlation between temperature distribution and rotor dynamics and, based on the analysis of the obtained data, set out to describe in detail how a lubricating film forms in a foil bearing.

2. Description of the Test Rig

The test rig consisted of several components, as shown in Figure 1. The electric motor (electrospindle) was connected to the shaft through a flexible coupling. The maximum rotational speed of the motor was 24,000 rpm. The shaft was supported by two foil bearings, and one of them (bearing No. 2) was modified so that the temperature and deformation of the top foil could be measured. The bearing with thermocouples (bearing No. 2) had its own special support to accommodate the necessary conductors. The diameter of the bearing journals was 30 mm. Vibration acceleration in three directions was measured on the bearing supports (Figure 1a). Eddy current sensors (positioned at a 45-degree angle to the shaft axis) and laser sensors, placed on additional supports, were used to measure displacement both in the Y direction (direction of the gravitational force) and X direction (direction opposite to the direction of the gravitational force). Two types of sensors were used to reduce the measurement error (Figure 1b). The axial displacement of the shaft was also recorded.
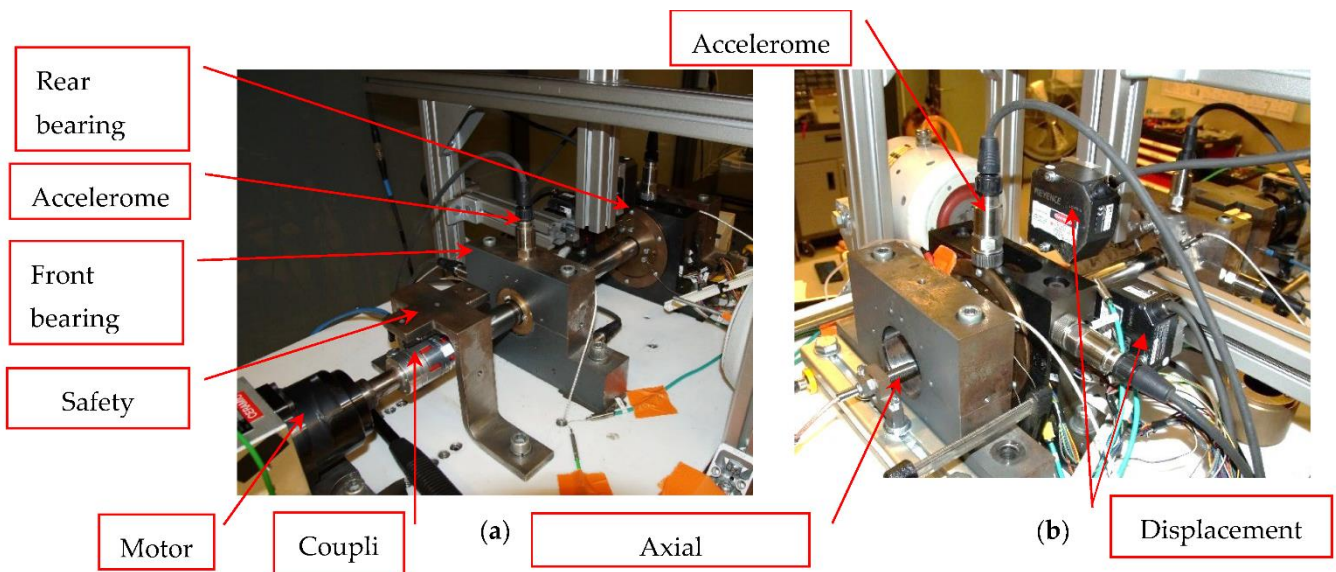
Rear bearing

Accelerome

Front bearing

Safety

Motor

Coupli

Accelerome

(a)

Axial

(b)

Displacement

Figure 1. (**a**) Front bearing support (front view); (**b**) Rear bearing support with measuring equipment (rear view).

In a traditional foil bearing, it is difficult to measure the temperature and deformation of the top foil. In the method used [16], which is based on contact between the thermocouple tip and the foil, there was uncertainty with regard to the correct connection between the temperature sensors and the surface of the foil. A decision was made to change the way the thermocouples were mounted and integrated into the foil (Figure 2a,b). This involved permanently connecting the temperature sensors on the outside of the top foil. The thermocouples were arranged on the foil, forming a 3 × 6 grid whose dimensions are shown in Figure 3a. Strain gauges were also welded to the foil. A detailed description of the entire installation procedure can be found in articles [17,18].
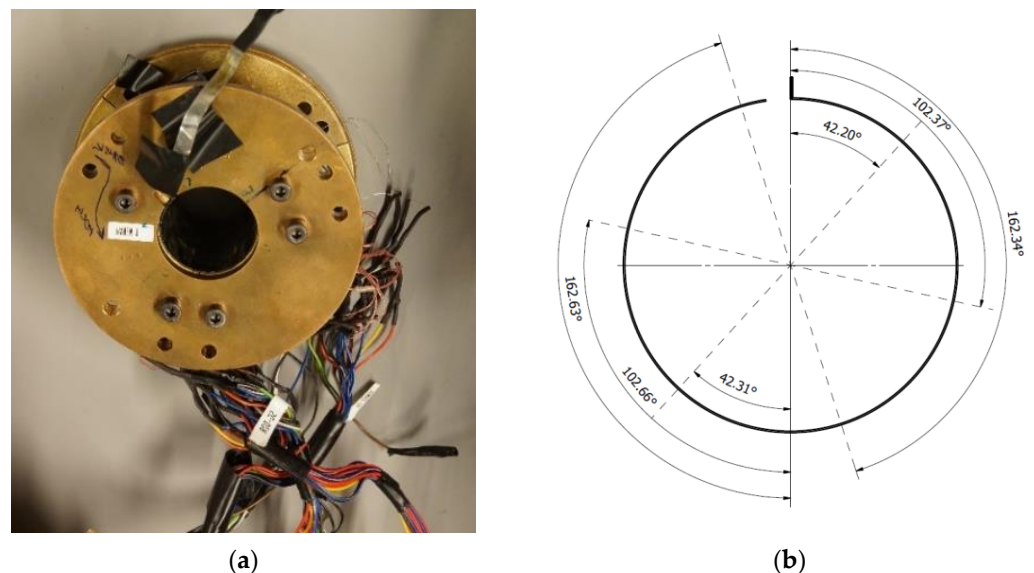
(a)

(b)

Figure 2. (**a**) Tested bearing (second bearing); (**b**) Angular thermocouple distribution on the top foil.

The foil bearing tested consisted of three bump foils and a single top foil made of Inconel 625. In addition, the top foil had been coated with a Teflon-based anti-friction material. The bearing had a nominal diameter of 30 mm and a width of 40 mm. The bump foil had notches, placed across its width, which allowed the passage of conductors towards the top foil (Figure 3b). The sleeve also had similar notches.
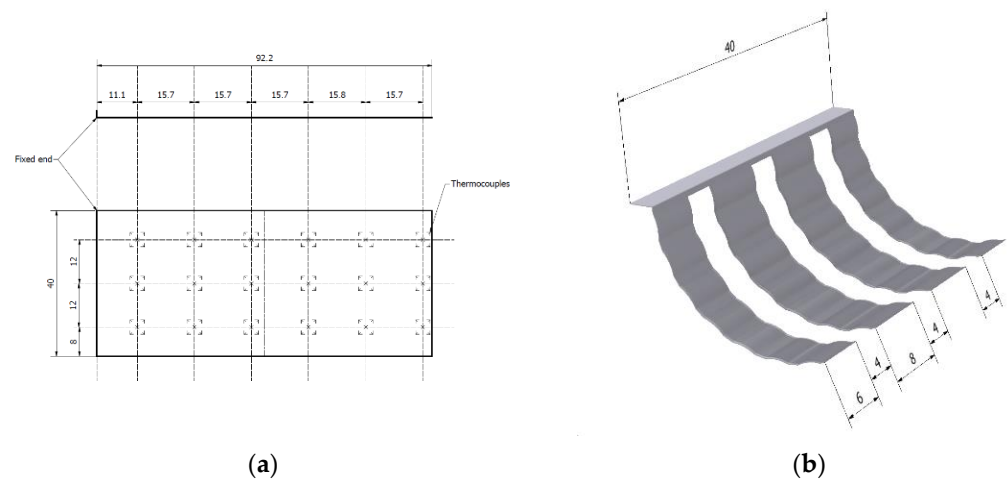
Figure 3. (**a**) Thermocouple distribution on the flat surface of the top foil; (**b**) CAD model of bump foil with notches.

3. Results

A number of tests had been carried out on the test rig described above. This article focuses mainly on the correlation between the temperature distribution on the top foil and the vibrations of the journal. For this purpose, a test was carried out by gradually reducing the rotor speed from the maximum speed to the lowest speed at which the bearings could operate, without destroying the anti-friction coating. The test consisted of: accelerating the rotor to a speed of 24,000 rpm (max. speed), running the rotor at a constant speed for about 200 s, and gradually decreasing the speed (by 2000 rpm). Each set rotational speed matched the vibration trajectories of the journal, and these affected the temperature distribution of the foil.

Figure 4 shows the position characteristics of the bearing journals, which started from a value of −20 µm because this value was taken as the value of the radial clearance. At zero speed (0 rpm), the bearing journals were displaced from the bearing axis by this distance. The pink colour indicates the moment when the measured values were read. The course of the rotational speed is marked in black. The red (X1) and green (Y1) colours indicate the displacement of the first journal in the X and Y directions, and the navy blue (X2) and turquoise (Y2) colours indicate the displacement of the second journal.
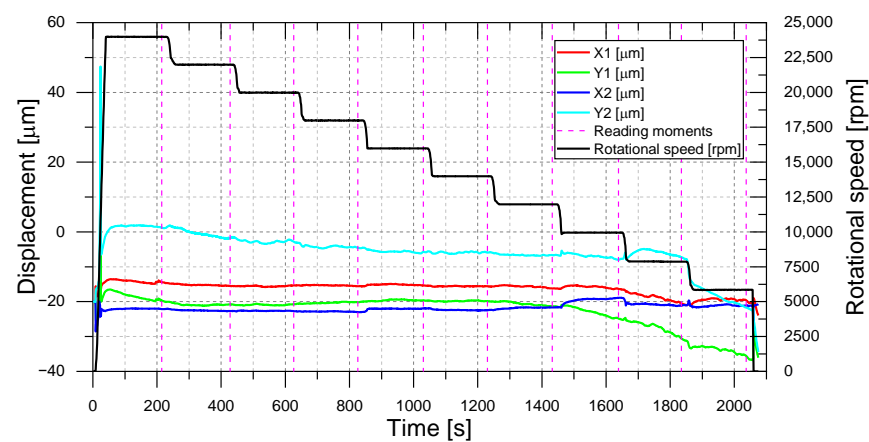

Figure 4. Rotational speed and radial displacement of the rotor versus time.

During the initial run-up period (Figure 5), up to a speed of 500 rpm, the first bearing journal changed its position by 5 µm and −5 µm in the X and Y directions, respectively, while the second bearing journal changed its position by −8 µm and 4 µm in the X and Y

directions, respectively. At a speed of 10,792 rpm, the displacements of the journals were as follows: X1—15 µm, Y1—0 µm, X2—−2 µm, Y2—67 µm. After the maximum speed was reached, the journals reached a steady state, in relation to the value of the radial clearance, with the following values: X1—5 µm, Y1—1 µm, X2—−2 µm, Y2—22 µm. As it could be observed, the second journal lifted itself higher than the first, which was held in place by the coupling.
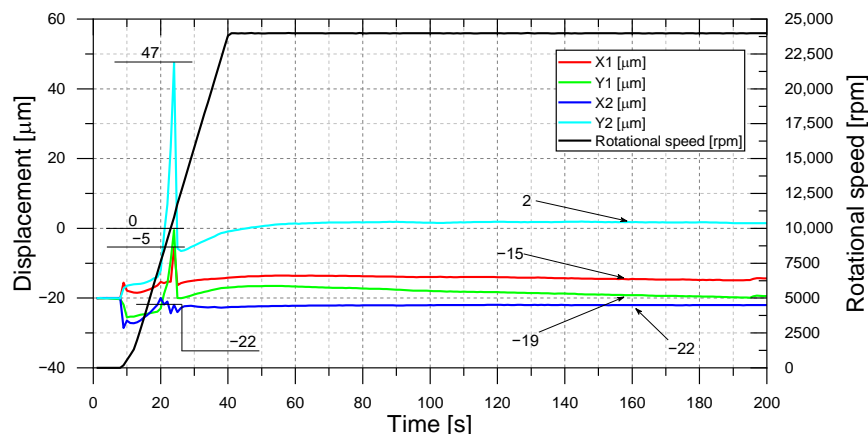

Figure 5. Rotational speed and radial displacement of the rotor versus time (first 200 s).

Figure 6 shows the position of the journals in both bearings, at different speeds, during a gradual run-down. The red dots indicate the positions of the journals in the bearings at a constant selected speed, and the green lines show the displacements of the journals in the bearing during the test. The word "start" marks the start of the test (at zero speed). The graphs have different scales to better illustrate the movement of the journals. Each of them was selected after a period of stable operation and marked on the graph shown in Figure 4. The journal of the first bearing operated close to one point from maximum speed up to about 12,000 rpm with a slight deviation in the direction perpendicular to the direction of the gravitational force (X). This region can be inscribed in a circle with a diameter of 3.5 µm. As the speed decreased, the journal dropped by −15 µm relative to the starting position. This kind of performance had already been observed and was largely associated with the use of a flexible coupling. The journal of the second bearing, where temperature was measured, behaved differently. With each lower set speed, it changed its position within the clearance circle until it reached a position close to the starting position. Up to a speed of 8000 rpm, it was within an area with a diameter of approximately 10 µm. In both cases, the speed reduction was followed by a lowering of the journals in the direction of the gravitational force. This was caused by the loss of the gas film [19].

The graphs presented in Figures 7–16 show the vibration trajectories obtained for each set rotational speed (filtered signal according to the rotational speed—1X). Figure 7 shows the vibration trajectories of both journals at a speed of approximately 24,000 rpm. For journal No. 1, the trajectory appears to be a counter-rotating flat ellipse with a major axis length of 4 µm. On the other hand, the concurrent trajectory of journal No. 2 was much larger and had dimensions of 9 × 6 µm. When the speed was reduced by 2000 rpm (Figure 8), both journals vibrated in the direction of rotation and the size and shape of the trajectories did not change significantly. The same occurred at 19,991 rpm and 17,990 rpm (Figures 9 and 10), except that the trajectory of the second journal was reduced by half. At a lower speed (Figure 11), the trajectory of the second journal almost doubled to about 8 µm and both of them were elliptical. At 13,988 rpm (Figure 12), the trajectory of the first journal increased to 10 µm and became circular, while the second journal did not change the nature of Its movement. Reducing the speed by about 2000 rpm resulted in a further increase in the trajectory of the first journal to a value of about 18 µm (Figure 13). At a speed of 9947 rpm (Figure 14), a twofold increase in the size of both trajectories was observed, and the trajectory of the first and the second journal increased to 40 and 10 µm, respectively.

In addition, the trajectory of the first journal became elliptical. When the rotational speed of the shaft decreased even further (Figure 15), both trajectories increased and reached a peak at 7867 rpm, 75 μm in the first bearing and 45 μm in the second. Both journals vibrated in opposite directions. At the lowest recorded speed of 5848 rpm (Figure 16), both trajectories rounded off and reached values of 32 and 9 μm for the first and the second journal, respectively.
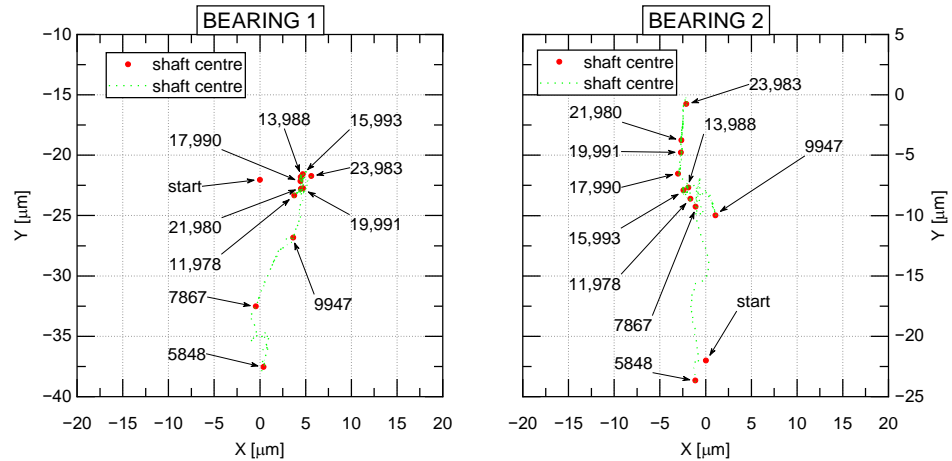

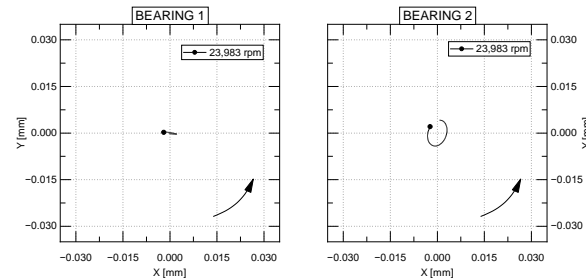**Figure 6.** Position of bearing journals in relation to rotational speed.

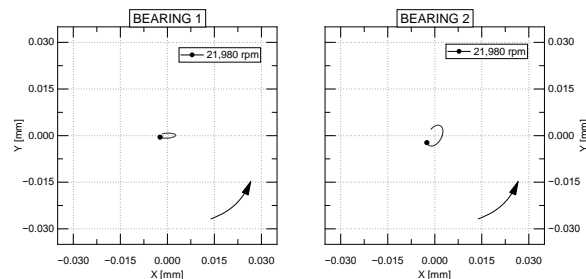**Figure 7.** Vibration trajectories of the two bearing journals at a speed of 23,983 rpm.

Figure 8. Vibration trajectories of the two bearing journals at a speed of 21,980 rpm.
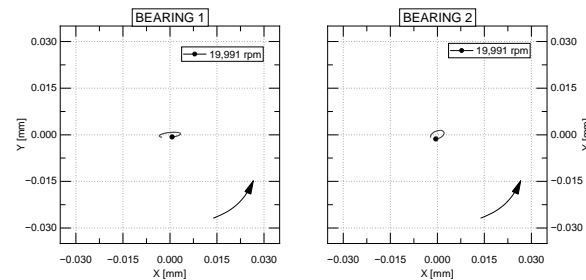

Figure 9. Vibration trajectories of the two bearing journals at a speed of 19,991 rpm.
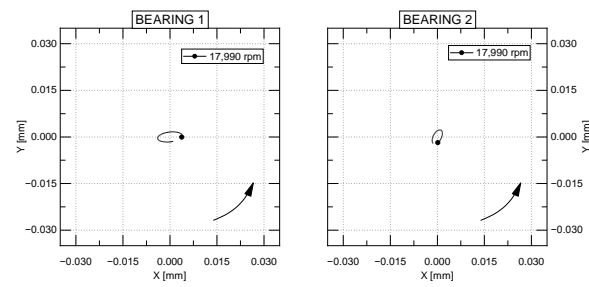
Figure 10. Vibration trajectories of the two bearing journals at a speed of 17,990 rpm.

Figure 11. Vibration trajectories of the two bearing journals at a speed of 15,993 rpm.

Figure 12. Vibration trajectories of the two bearing journals at a speed of 13,988 rpm.

Figure 13. Vibration trajectories of the two bearing journals at a speed of 11,978 rpm.
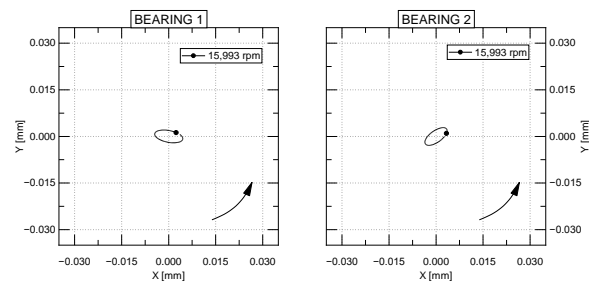

Figure 14. Vibration trajectories of the two bearing journals at a speed of 9947 rpm.
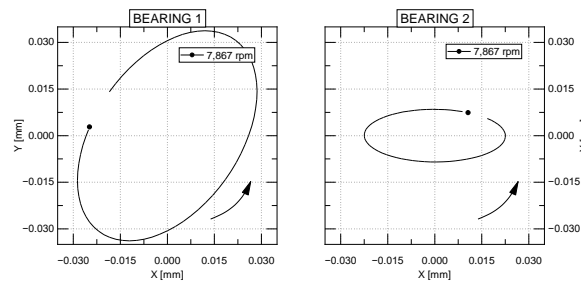
Figure 15. Vibration trajectories of the two bearing journals at a speed of 7867 rpm.
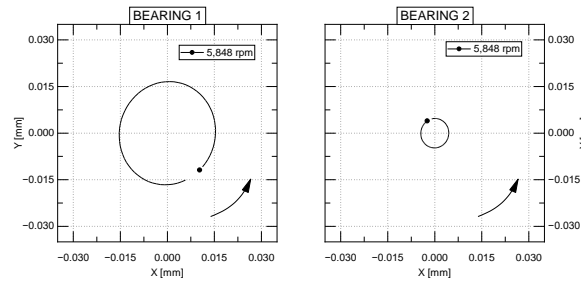
Figure 16. Vibration trajectories of the two bearing journals at a speed of 5848 rpm.
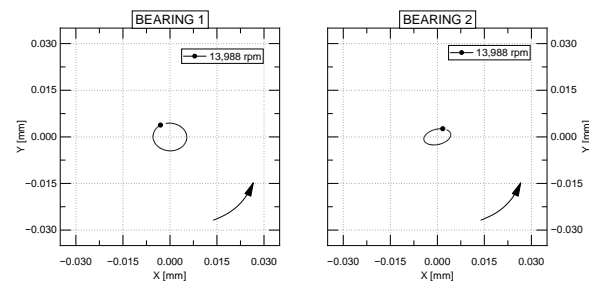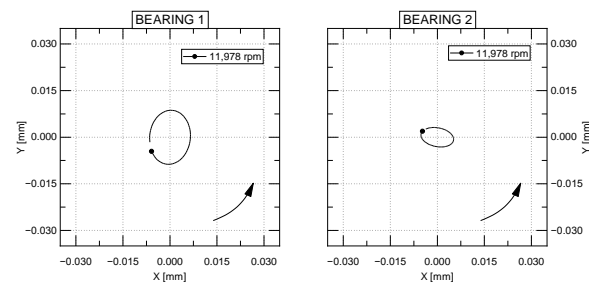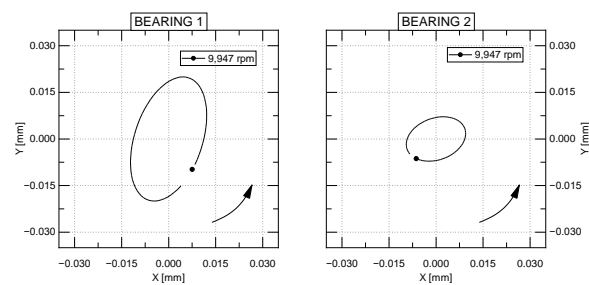
Figures 17 and 18 show temperature waveforms recorded at different rotational speeds. The decision was made to divide the characteristics according to the position of the thermocouples across the width of the foil. In the designations of thermocouples (TC), the symbol "_" is followed by the distance from the lock of the top foil (along its length), and the next number, which is written after the hyphen, indicates the distance from one of the edges of the foil (Figure 2b).

(**a**)

(**b**)

Figure 17. Temperature recorded on the top foil along its length versus rotational speed: (**a**) at a distance of 8 mm from the edge of the foil; (**b**) at a distance of 20 mm from the edge of the foil.

Figure 18. Temperature recorded on the top foil along its length versus rotational speed (at a distance of 32 mm from the edge of the foil).

Thermocouples labelled "TC_26.8-8", "TC_26.8-20" and "TC_26.8-20" were observed to show the lowest temperature, regardless of operating conditions. In addition, the sensors placed in the last rows indicated a certain degree of symmetry.
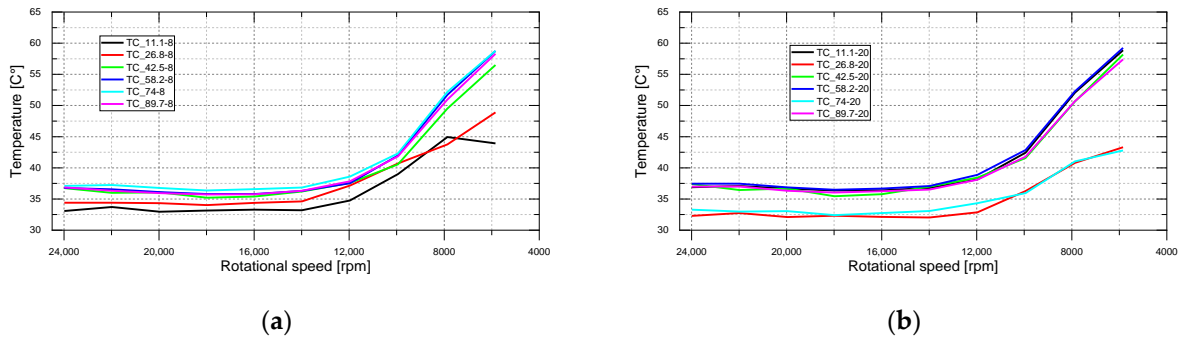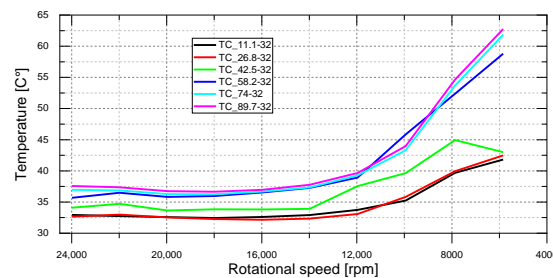
4. Analysis of the Results

In order to comprehensively analyze the relationship between journal movement and temperature, the decision was made to match the temperatures collected at the points and place them on the surface of the top foil. For this purpose, in the first step, the temperature values obtained at the highest speed were shown depending on the width of the foil in Figure 19a. Then, the temperature variation across the whole width of the foil for all columns of sensors (TC) was fitted using polynomial curves (in this case, second-order polynomials were used as they best reflected the nature of the distribution). This method followed the approach proposed in the article [20]. The curves along the length have been presented in a similar manner to Figure 19b, but in this case, the best fit guaranteed a fifth-order polynomial. As can be seen, the temperature values close to the lock (at the localization marked as 0 mm) were estimated to be too high, so they were discarded. Probably, if an additional column of thermocouples (placed closer to the foil lock) had been used, a more accurate fit would have been achieved. In order to find out about the fit of the curves to the point values, the statistical measure called R-squared was used to qualify the linear regression manifested by the percentage fit of the curves to the given values. R-squared is usually between 0 and 1, where 1 means a perfect representation. In our case, for all rotational speeds, the R-square coefficient was 1. In the literature, one can find the results of numerical calculations where the temperature is evenly distributed along the length of the top foil [21] and in some cases the temperature distribution of the top foil clearly reflects the shape of the bump foil. The peak temperature values on the top foil are at the apex of the convexity of the bump foil, while the temperature minima correspond to the segments between the bumps [15,22].
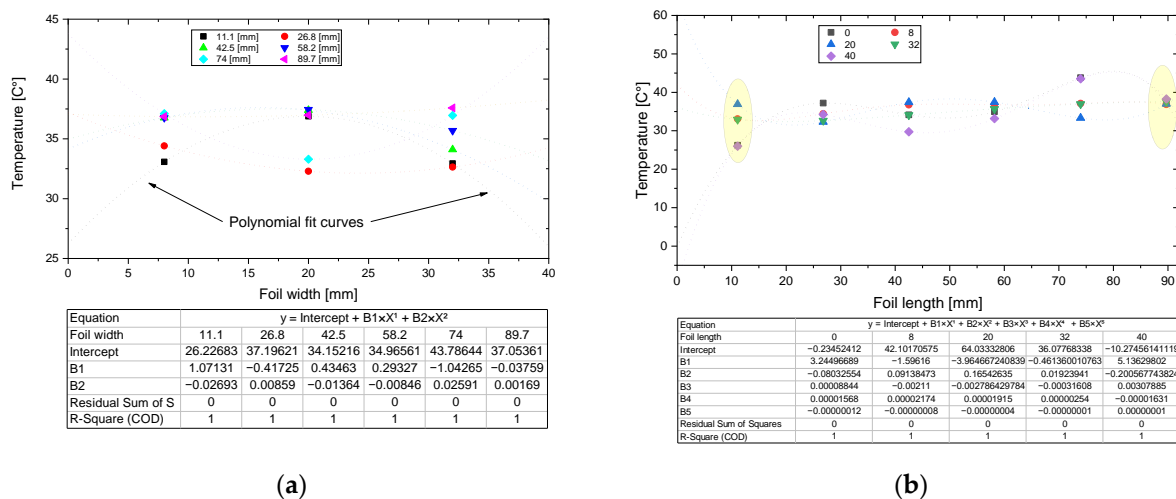

Equation	y = Intercept + B1×X^1 + B2×X^2					
Foil width	11.1	26.8	42.5	58.2	74	89.7
Intercept	26.22683	37.19621	34.15216	34.96561	43.78644	37.05361
B1	1.07131	−0.41725	0.43463	0.29327	−1.04265	−0.03759
B2	−0.02693	0.00859	−0.01364	−0.00846	0.02591	0.00169
Residual Sum of S	0	0	0	0	0	0
R-Square (COD)	1	1	1	1	1	1

(**a**)

Equation	y = Intercept + B1×X^1 + B2×X^2 + B3×X^3 + B4×X^4 + B5×X^5				
Foil length	0	8	20	32	40
Intercept	−0.23452412	42.10170575	64.03332806	36.07768338	−10.27456141119
B1	3.24496689	−1.59616	−3.96467240839	−0.46136010763	5.13629802
B2	−0.08032554	0.09138473	0.16542635	0.01923941	−0.200567743824
B3	0.00008844	−0.00211	−0.002786429784	−0.00031608	0.00307885
B4	0.00001568	0.00002174	0.00001915	0.00000254	−0.00001631
B5	−0.00000012	−0.00000008	−0.00000004	−0.00000001	0.00000001
Residual Sum of Squares	0	0	0	0	0
R-Square (COD)	1	1	1	1	1

(**b**)

Figure 19. Temperature distribution curves fitted to temperature values obtained from measurement points distributed along: (**a**) the width of the top foil; (**b**) the length of the top foil.

The presented method overestimates the temperature values close to the lock, but it describes the temperature distribution between the measurement points with good accuracy. The next step was to match the two-dimensional temperature results obtained (Figure 19) to the surface of the top foil. In order to better reflect the temperature changes, an average value of the nearby measurement points (which are marked in yellow on the right side of Figure 19) was set in the foil lock (0 mm). This was based on the results described in the article [13], where the temperature close to the fixed end was close to the value at the free

end of the top foil. A polynomial surface with a specified degree in x and y was used to illustrate the temperature distribution on the surface, according to the following formula:

$$P_{i,j}(x,y) = c_{00} + c_{10}x + c_{01}y + c_{20}x^2 + c_{11}xy + c_{02}y^2 + c_{30}x^3 + c_{21}x^2y + c_{12}xy^2 \quad (1)$$

where 10 is the maximum value of *i* and *j*; *i* and *j* stand for the foil width and length, respectively.

In each case, the best fit was obtained using the polynomial $P_{2,7}(x,y)$, and the R-squared coefficient ranged from 0.94 to 0.99. Below, examples of temperature distributions obtained at maximum (Figure 20a) and minimum (Figure 20b) rotational speed are shown.
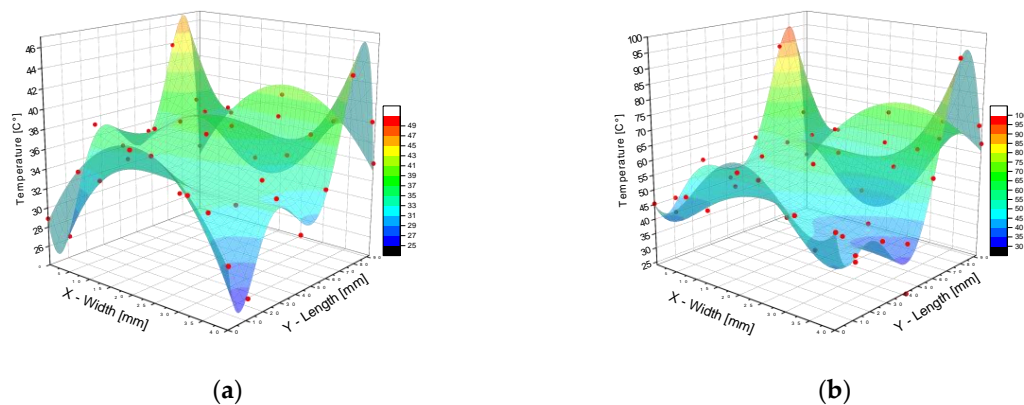

(**a**)　　　　　　　　　　　　　　　　　　　　　(**b**)

Figure 20. Temperature distribution on the flat surface of the top foil at: (**a**) maximum speed; (**b**) minimum speed.

Different scales have been used to better illustrate the temperature distribution on the foil surface. The red dots indicate the measurement points enriched with temperature values at the edges of the foil, which were determined using a 2D method. In both cases of extreme speeds, the highest temperature occurs at the edges of the foil, close to the free end. This means that the lubrication gap was too small in this area, and this was caused, for example, by excessive pressure on the top foil exerted by the bump foil. Such a phenomenon could have caused local rubbing of the top foil against the journal.

Figures 21–25 show the obtained temperature distributions on the top foil, as well as the vibration trajectory at a given rotational speed. The vibration trajectories of the second journal are shown and described in more detail in Figures 11–16. This foil was modelled as a perfectly cylindrical surface and its lock was at the top (at the location 0 mm). The position of the journal is not taken into account in the figures because it would be difficult to visualize, but in their descriptions it is indicated in the order X and Y, counting from the bearing axis. The two-dimensional trajectory is in the plane of symmetry of the bearing (red colour) and its scale is on the back plane. In Figure 21a,b, similar temperature values were observed but slightly different temperature distributions, probably due to the different positions of the journal in the bearing.

Along with a different static equilibrium point, at a given rotational speed, the size of the trajectory also decreased, which translated into slight differences (Figure 22a,b). In each case, in the lower part of the foil, in the middle of its width, an area of higher temperature can be seen, while in the middle, near the penultimate column of thermocouples, there is an area of low temperature (near the free end).

In the upper part of the top foil, on the lock side, an area of increased temperature is observed, with much lower values at the edges, which may be related to the suction of air from the environment. At these four analyzed speeds, the distribution appears to be symmetrical, which is related to the nature of the operation of the entire rotor.

At lower speeds (Figure 23a,b), the vibration trajectories enlarged slightly and the journals reached the static equilibrium position farther from the bearing axis than at 23,983 rpm. The temperature values remained at a similar level but the nature of the temperature distribution changed. The area of lower temperature, located closer to the

free end of the foil, remained unchanged but in the lower part of the foil, the temperature distribution lost its symmetry. This effect is due to several factors: the shape of the ellipse, and the direction of the major axis directed to the location of the higher temperature area; the position of the journal in the bearing; the emerging eccentricity of the journals of the bearings; and the developing conical vibration mode of the rotor.
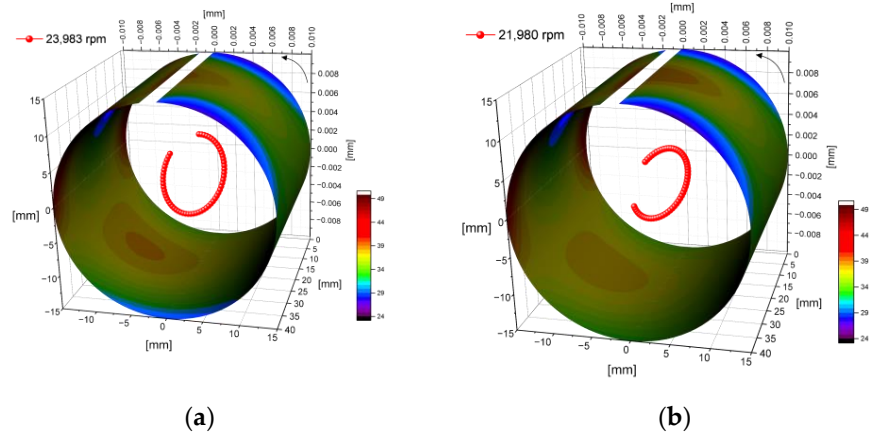

(**a**)   (**b**)

Figure 21. Temperature distribution on the surface of the top foil and the vibration trajectory of the journal: (**a**) at the speed of 23,983 rpm (−2 μm, −1 μm), (**b**) at the speed of 21,980 rpm (−3 μm, −4 μm).

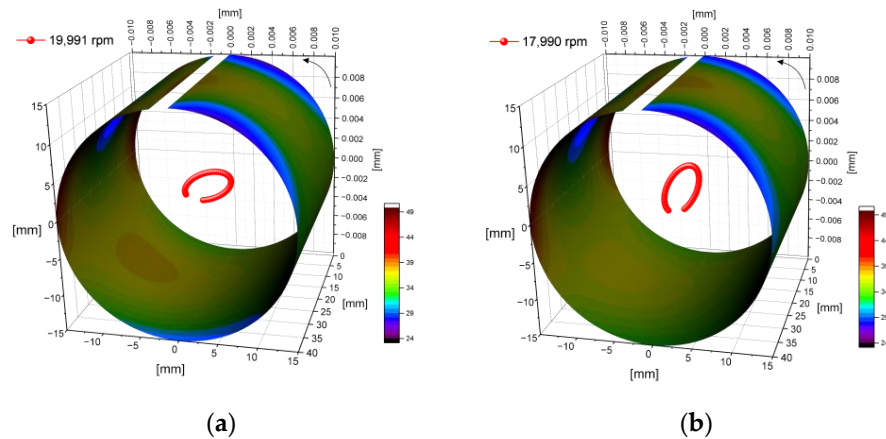(**a**)   (**b**)

Figure 22. Temperature distribution on the surface of the top foil and the vibration trajectory of the journal: (**a**) at the speed of 19,991 rpm (−3 μm, −5 μm), (**b**) at the speed of 17,990 rpm (−3 μm, −7 μm).

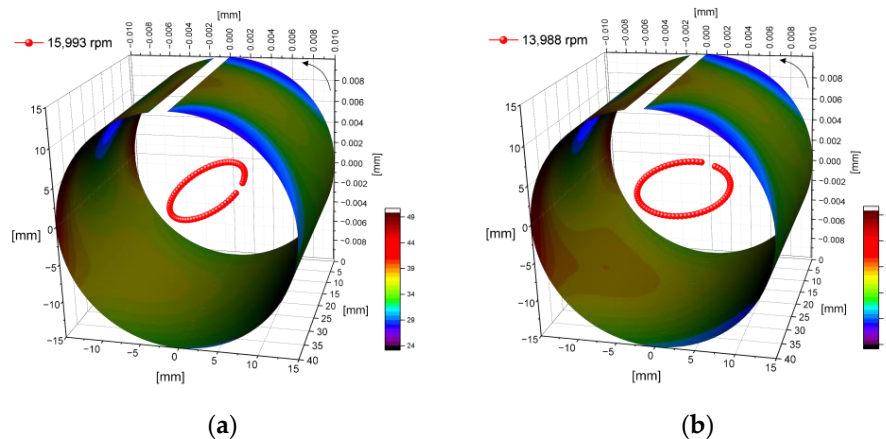(**a**)   (**b**)

Figure 23. Temperature distribution on the surface of the top foil and the vibration trajectory of the journal: (**a**) at the speed of 15,993 rpm (−2 μm, −8 μm), (**b**) at the speed of 13,988 rpm (−2 μm, −8 μm).

Figure 24. Temperature distribution on the surface of the top foil and the vibration trajectory of the journal: (**a**) at the speed of 11,978 rpm (−2 μm, −9 μm), (**b**) at the speed of 9947 rpm (−1 μm, −10 μm).
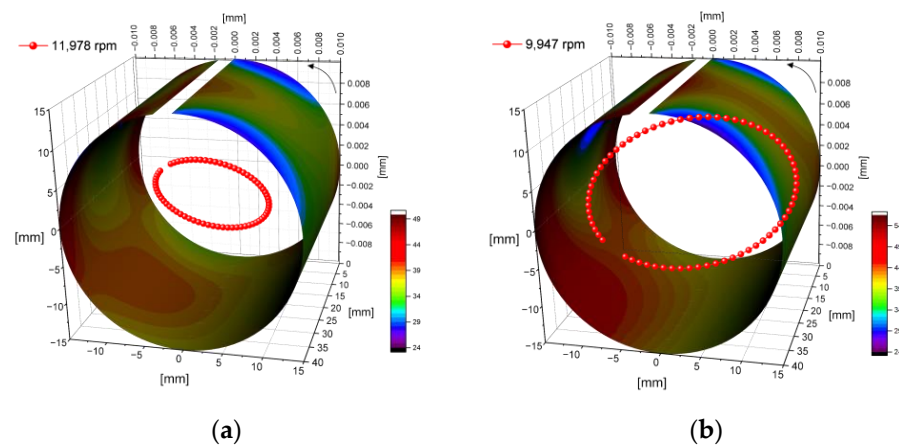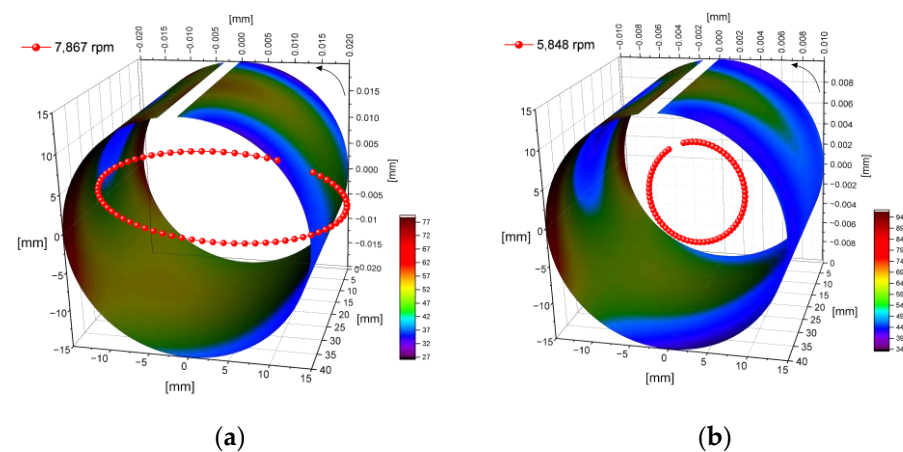

Figure 25. Temperature distribution on the surface of the top foil and the vibration trajectory of the journal: (**a**) at the speed of 7867 rpm (−1 μm, −9 μm), (**b**) at the speed of 5848 rpm (−1 μm, −24 μm).

In Figure 6, it can be seen that at speeds of 15,993 rpm and 13,988 rpm, the difference in the positions of both journals is 13 μm while in Figure 12, it can be observed that the vibration mode of the rotor took a conical form.

As the rotational speed decreased to 11,978 rpm (Figure 24a), the elliptical trajectory of the journal vibrations increased and its major axis rotated nearly perpendicular to the lock of the top foil. The journal slightly changed its position and there was still a 13 μm eccentricity with a conical vibration mode of the rotor. In the upper part of the foil, at its visible edges as well as at the free end, the low-temperature area increased. The maximum temperature reached almost 50 °C, which means an increase of about 5 °C compared to the higher speeds. The highest temperature was no longer near the lock and the edge of the free end, but at the edges of the foil according to the shape of the trajectory. As the rotational speed decreased to 9947 rpm (Figure 24b), the conical form enlarged while the eccentricity of the journals increased to 17 μm. This resulted in an increase in the maximum temperature to 54 °C, which occurred on the left side of the foil except for the area in the middle, closer to the lock (as at higher speeds). As the air film became thinner and thinner, the temperature values increased in the plane of symmetry of the foil across its entire width.

At the speed of 7867 rpm (Figure 25a), where the lubricating film was assumed to be absent or very thin, the journal trajectory had doubled its vibration amplitude (as seen on the scale). In the plane of symmetry of the foil, the average temperature was about 55 °C, except for the area located on the left side of the foil. The journal sucked cool air into the space between the journal and the foil at the bottom of the bearing. The enlarged area in the upper left part of the foil indicated that friction was already occurring between

the journal and the top foil, causing its free end to be stretched (pulled back) towards the bearing sleeve. Such a fact causes the cool air to be sucked from the space between the lock and the free end of the foil and enters the area located in the upper left part. On the other hand, the nature of the operation of the journal worsens the cooling of the lower part of the bearing because the highest friction occurred there. The highest temperature occurred at the edges of the foil because that is where the gas film was thinnest or no longer exists.

The highest temperatures were recorded when the set rotational speed was lowest (Figure 25b). The journal was already lying on the foil, rotating with a trajectory four times smaller. Hence, the highest temperature was recorded in the lower part of the bearing, and the taut top foil (approaching the sleeve) creates a space for cool air to enter.

5. Discussion

To evaluate the temperature and performance of the rotor, two bearings with the same geometry were used. One of them had the top foil modified and thermocouples and strain gauges were welded to it. This article focuses on the temperature distribution, without taking into account the deformation, which is the subject of study in other papers. The temperature measurement method that was used seems to be reliable. Of course, welding the measuring elements on the outside of the top foil changes its stiffness and other properties, but the foil bearing showed no disturbing signs of malfunctioning compared to the other bearing. The specially designed bump foil also helped with this.

Basic dynamic parameters of the rotor journals, such as vibration trajectories and displacements of the journals in the bearings, were obtained. The vibration trajectory was filtered to 1X, which made it very easy to interpret the results. Eighteen thermocouples were welded on the surface of the top foil, which made it possible to obtain fairly good measurement resolution for the purpose of evaluating the correct operation of the foil bearing. To study the temperature distribution on the foil, either a larger number of measurement points or some approximation of the recorded data was needed. The best match across the width of the top foil was obtained using a second-order polynomial, and along the length, using a seventh-order polynomial (assuming that the temperature near the lock of the foil is the average of the points in the vicinity). Assuming that such curves and approximations describe well the temperature distribution on the top foil, an attempt was made to make the temperature distribution dependent on the rotor dynamics (that is the movement of the bearing journal).

In the center of the bearing (plane of symmetry across the width of the top foil), the highest temperature value was expected, propagating to smaller values located at the edges. Such a symmetrical distribution was noticeable when the journals were close to the axis of the bearing sleeves, otherwise, the distribution across the width of the top foil became asymmetrical. This phenomenon can be effectively observed by comparing the temperature distribution and journal positions in the bearing at a given rotational speed. Thus, the symmetry of the foil temperature distribution depends strongly on the form of vibration of the entire rotor.

No obvious correlation was observed between the size of the vibration trajectory and the value or temperature distribution because the flexible set of foils adapts itself to the size of the trajectory. This becomes different, however, when considering the size and shape of the trajectory. Some correlations can be observed between the shape of the vibration trajectory of the journal and the temperature distribution along the length of the top foil, and thus the gas exchange in the lubrication gap, but this is not unequivocal. Such phenomena cannot be observed on the built test rig, as it would be necessary to change the size of the trajectory and its shape under constant operating conditions in terms of journal position and rotational speed. This would require controlling the unbalance, stiffness and damping of the set of foils. In the case described herein, the vibration trajectory of the journal is associated with a given rotational speed, which causes the displacement of the high- and low-temperature areas.

Another interesting finding is that when the lubricating film is lost, the rotating journal, located on the top foil, creates a space for air to enter into the lubrication gap. This is caused by the weight of the rotor, which exerts pressure on the surface of the foil, and by viscous friction, which stretches the foil in the opposite direction to the lock. In the case of the rotational speed at which there is no lubricating film, an important aspect of this phenomenon is the size and shape of the vibration trajectory, which affects the entry of air into the foil bearing. This explains how the formation of a lubricating film can proceed in a foil bearing.

The results presented herein have made it possible to observe from which bearing spaces the air is sucked in to form the lubricating film. At low rotational speeds, before the formation of the lubricating film, the journal draws in cool air from the space of the lock and the free end of the foil and from the areas located near the edge of the top foil, i.e., the areas located halfway along the length of the edge of the foil, counting in the direction of rotation. As the rotational speed increases, the area of cooling air supply decreases and is located at the foil lock (approximately a quarter of the foil length, counting in the direction of rotation). At high speeds, the air supply from the side of the space of the lock and the free end of the top foil is limited by the edge of the free end of the foil because it is pulled towards the journal, as can be seen on the temperature distribution graph (the temperature at this edge is high).

In some cases, at high speeds, the vibration trajectory forces an additional area to appear, from which the journal draws in cool air. It is mainly located in the lower part of the bearing, in the areas where the same temperatures occur at near the lock of the top foil.

6. Conclusions

- ○ Welding of temperature sensors to the top foil has no significant impact on the operation of the foil bearing.
- ○ Eighteen temperature measuring points located on the top foil are sufficient to estimate the temperature distribution, but it is recommended to double the number of thermocouples.
- ○ The temperature distribution on the top foil can be described using a polynomial.
- ○ The symmetry of the foil temperature distribution strongly depends on the vibration shape of the entire rotor.
- ○ The size of the trajectory has no significant effect on the temperature distribution when the bearing is operating at nominal speed.
- ○ During the formation of a lubricating film, the shape and size of the vibration trajectory are important factors to be taken into account.

Institutional Review Board Statement: Not applicable.

Informed Consent Statement: Not applicable.

Data Availability Statement: Not applicable.

Conflicts of Interest: The authors declare no conflict of interest.

References

1. Choe, B.S.; Kim, T.H.; Kim, C.H.; Lee, Y.B. Rotordynamic Behavior of 225 KW (300 HP) Class PMS Motor–Generator System Supported by Gas Foil Bearings. *J. Eng. Gas Turbines Power* **2015**, *137*, 092505. [CrossRef]
2. Sim, K.; Lee, Y.B.; Song, J.W.; Kim, J.B.; Kim, T.H. Identification of the Dynamic Performance of a Gas Foil Journal Bearing Operating at High Temperatures. *J. Mech. Sci. Technol.* **2014**, *28*, 43–51. [CrossRef]
3. Feng, K.; Liu, Y.; Zhao, X.; Liu, W. Experimental Evaluation of the Structure Characterization of a Novel Hybrid Bump-Metal Mesh Foil Bearing. *J. Tribol.* **2015**, *138*, 021702. [CrossRef]
4. Żywica, G.; Bagiński, P.; Andrearczyk, A. A New Method of Manufacturing a Foil Bearing Using Tools Made by the Rapid Prototyping Technology. *CIRP J. Manuf. Sci. Technol.* **2020**, *31*, 514–524. [CrossRef]
5. Laskowski, J.A.; Della Corte, C. Friction and Wear Characteristics of Candidate Foil Bearing Materials From 25 °C to 800 °C. *Lubr. Eng.* **1996**, *52*, 605–616.
6. San Andres, L.; Jung, W. Evaluation of Coated Top Foil Bearings: Dry Friction, Drag Torque, and Dynamic Force Coefficients. *Circ. J.* **2004**, *68*, 845.
7. Baum, C.; Hetzler, H.; Schröders, S.; Leister, T.; Seemann, W. A Computationally Efficient Nonlinear Foil Air Bearing Model for Fully Coupled, Transient Rotor Dynamic Investigations. *Tribol. Int.* **2021**, *153*, 106434. [CrossRef]
8. Zhang, W.; Alahyari, A.A.; Chiappetta, L. A Fully Coupled Fluid–Structure Interaction Model for Foil Gas Bearings. *J. Eng. Gas Turbines Power* **2016**, *139*, 022501. [CrossRef]
9. Kim, T.H.; Andrés, L.S. Limits for High-Speed Operation of Gas Foil Bearings. *J. Tribol.* **2006**, *128*, 670–673. [CrossRef]
10. Hou, Y.; Chen, S.; Chen, R.; Zhang, Q.; Zhao, H. Numerical Study on Foil Journal Bearings with Protuberant Foil Structure. *Tribol. Int.* **2011**, *44*, 1061–1070. [CrossRef]
11. Park, J.; Kim, D.; Sim, K. Development and Performance Measurements of Gas Foil Polymer Bearings with a Dual-Rotor Test Rig Driven by Permanent Magnet Electric Motor. *Appl. Sci.* **2022**, *12*, 1505. [CrossRef]
12. Ryu, K.; San Andrés, L. On the Failure of a Gas Foil Bearing: High Temperature Operation Without Cooling Flow. *J. Eng. Gas Turbines Power* **2013**, *135*, 112506. [CrossRef]
13. Sim, K.; Lee, Y.B.; Song, J.W.; Kim, T.H. Effect of Cooling Flow on Thermal Performance of a Gas Foil Bearing Floating on a Hot Rotor. *J. Mech. Sci. Technol.* **2018**, *32*, 1939–1954. [CrossRef]
14. Bagiński, P.; Żywica, G.; Lubieniecki, M.; Roemer, J. The Effect of Cooling the Foil Bearing on Dynamics of the Rotor-Bearings System. *J. Vibroeng.* **2018**, *20*, 843–857. [CrossRef]
15. Mahner, M.; Bauer, M.; Schweizer, B. Numerical Analyzes and Experimental Investigations on the Fully-Coupled Thermo-Elasto-Gasdynamic Behavior of Air Foil Journal Bearings. *Mech. Syst. Signal Process.* **2021**, *149*, 107221. [CrossRef]
16. Zywica, G.; Baginski, P.; Banaszek, S. Experimental Studies on Foil Bearing With a Sliding Coating Made of Synthetic Material. *J. Tribol.* **2015**, *138*, 011301. [CrossRef]
17. Zdziebko, P.; Martowicz, A. Study on the Temperature and Strain Fields in Gas Foil Bearings–Measurement Method and Numerical Simulations. *Eksploat. Niezawodn. Maint. Reliab.* **2021**, *23*, 540–547. [CrossRef]
18. Martowicz, A.; Roemer, J.; Zywica, G. Thermal Characterization of a Gas Foil Bearing—A Novel Method of Experimental Identification of the Temperature Field Based on Integrated Thermocouples Measurements. *Sensors* **2022**, *22*, 5718. [CrossRef]
19. Mahner, M.; Bauer, M.; Lehn, A.; Schweizer, B. An Experimental Investigation on the Influence of an Assembly Preload on the Hysteresis, the Drag Torque, the Lift-off Speed and the Thermal Behavior of Three-Pad Air Foil Journal Bearings. *Tribol. Int.* **2019**, *137*, 113–126. [CrossRef]
20. Zhou, Y.; Shao, L.; Zhao, S.; Zhu, K.; Ding, S.; Du, F.; Xu, Z. An Experimental Investigation into the Thermal Characteristics of Bump Foil Journal Bearings. *Symmetry* **2022**, *14*, 878. [CrossRef]
21. Ryu, K.; Andrés, L.S. Effect of Cooling Flow on the Operation of a HotRotor-Gas Foil Bearing System. *J. Eng. Gas Turbines Power* **2012**, *134*, 102511. [CrossRef]
22. Zhang, K.; Zhao, X.; Feng, K.; Zhao, Z. Thermohydrodynamic Analysis and Thermal Management of Hybrid Bump–Metal Mesh Foil Bearings: Experimental Tests and Theoretical Predictions. *Int. J. Therm. Sci.* **2018**, *127*, 91–104. [CrossRef]